Hindawi
Journal of Nanomaterials
Volume 2017, Article ID 8792567, 9 pages
https://doi.org/10.1155/2017/8792567

Research Article

Gas Sensing Properties of $NiSb_2O_6$ Micro- and Nanoparticles in Propane and Carbon Monoxide Atmospheres

Verónica-M. Rodríguez-Betancourtt,[1] Héctor Guillén Bonilla,[2] Martín Flores Martínez,[2] Alex Guillén Bonilla,[3] J. P. Moran Lazaro,[3] José Trinidad Guillen Bonilla,[4] M. A. González,[5] and María de la Luz Olvera Amador[6]

[1]*Departamento de Química, CUCEI, Universidad de Guadalajara, 44410 Guadalajara, JAL, Mexico*
[2]*Departamento de Ingeniería de Proyectos, CUCEI, Universidad de Guadalajara, 44410 Guadalajara, JAL, Mexico*
[3]*Departamento de Ciencias Computacionales e Ingenierías, CUVALLES, Universidad de Guadalajara, Carretera Guadalajara-Ameca Km 45.5, 46600 Ameca, JAL, Mexico*
[4]*Departamento de Electrónica y Computación, CUCEI, Universidad de Guadalajara, 44410 Guadalajara, JAL, Mexico*
[5]*CONACYT, University of Guadalajara, CUCEI, Blvd. Marcelino García Barragán 1421, Ciudad Universitaria, 44430 Guadalajara, Jal, Mexico*
[6]*Departamento de Ingeniería Eléctrica-SEES, Centro de Investigación y de Estudios Avanzados del Instituto Politécnico Nacional, 07360 México City, Mexico*

Correspondence should be addressed to Alex Guillén Bonilla; alexguillenbonilla@gmail.com

Received 4 January 2017; Revised 12 April 2017; Accepted 18 April 2017; Published 7 June 2017

Academic Editor: Balachandran Jeyadevan

Micro- and nanoparticles of $NiSb_2O_6$ were synthesized by the microwave-assisted colloidal method. Nickel nitrate, antimony chloride, ethylenediamine, and ethyl alcohol were used. The oxide was obtained at 600°C and was analyzed by X-ray diffraction (XRD) and Raman spectroscopy, showing a trirutile-type structure with cell parameters $a = 4.641$ Å, $c = 9.223$ Å, and a space group $P4_2/mnm$ (136). Average crystal size was estimated at ~31.19 nm, according to the XRD-peaks. The microstructure was scrutinized by scanning electron microscopy (SEM), observing microrods measuring ~3.32 μm long and ~2.71 μm wide, and microspheres with an average diameter of ~8 μm; the size of the particles shaping the microspheres was measured in the range of ~0.22 to 1.8 μm. Transmission electron microscopy (TEM) revealed that nanoparticles were obtained with sizes in the range of 2 to 20 nm (~10.7 nm on average). Pellets made of oxide's powders were tested in propane (C_3H_8) and carbon monoxide (CO) atmospheres at different concentrations and temperatures. The response of the material increased significantly as the temperature and the concentration of the test gases rose. These results show that $NiSb_2O_6$ may be a good candidate for gas sensing applications.

1. Introduction

The detection of toxic and nontoxic gases has been of great importance for environmental protection and for its potential domestic and industrial applications [1]. Among the gases of which there is a broad interest for being monitored are oxygen (O_2), carbon monoxide (CO), carbon dioxide (CO_2), sulfur dioxide (SO_2), nitrogen oxides (NO and NO_2), hydrogen sulfide (H_2S), methane (CH_4), ethanol (C_2H_5OH), and propane (C_3H_8) [2–5]. Some oxides have been applied for the detection of different gases. Among them are semiconductors such as SnO, ZnO, Cr_2O_3, Mn_2O_3, NiO, CuO, SrO, In_2O_3, WO_3, TiO_2, V_2O_3, Fe_2O_3, and SnO_2 [6, 7], as well as the compounds $LaFeO_3$, $Mo_6S_3I_6$, and $CuCrO_2$ [8–10]. These materials are nowadays considered as extraordinary gas detectors because they possess good physical and chemical stability in different atmospheres.

Recently, some authors have placed great emphasis on the study of materials capable of detecting propane (C_3H_8) and carbon monoxide (CO) at different concentrations and

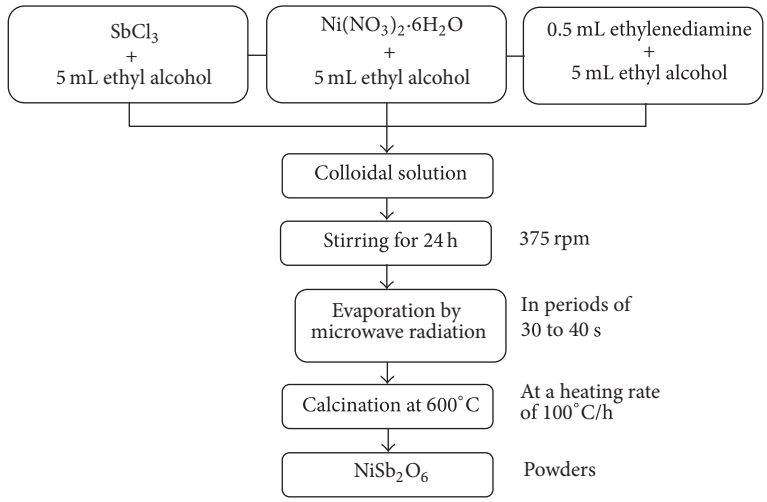

Figure 1: Schematic representation of the experimental steps used in the preparation of $NiSb_2O_6$ powders.

operating temperatures [5]. ZnO and SnO_2 are the most commonly used oxides to detect C_3H_8 and CO because they possess good thermal stability in these gases [11, 12]. The semiconductor oxides $LaCoO_3$ and $CoSb_2O_6$ are currently investigated as detectors of C_3H_8 and CO, showing good stability and a high response at moderate temperatures (between 250 and 350°C) [13, 14]. It is believed that the good response of these materials is largely due to the morphology and the nanometric size of the obtained particles. In fact, the response of any material used as gas detector is highly related to the morphology, the porosity, and the particle size; such microstructural features determine the efficiency of the chemical interaction between the gas molecules and the surface of the detecting material [15]. It is therefore of great importance (especially from an economic point of view) to achieve synthesis methods of materials with optimal morphologies and high efficiency. In this work, the microwave-assisted colloidal method was successfully used to synthesize micro- and nanoparticles of $NiSb_2O_6$ with great ability to detect different concentrations of carbon monoxide (CO) and propane (C_3H_8) at moderate temperatures.

2. Materials and Methods

2.1. Synthesis of $NiSb_2O_6$ Powders. The $NiSb_2O_6$ powders were prepared through the microwave-assisted colloidal method with 1.28 g of $Ni(NO_3)_2{\cdot}6H_2O$ (Mallinckrodt Beker, 99%) and 2.28 g of $SbCl_3$ (Sigma-Aldrich ≥ 99%), dissolved each in 5 mL of ethyl alcohol (CTR) and 0.5 mL of ethylenediamine (Sigma-Aldrich ≥ 99%). A colloidal solution was obtained, which was stirred for 24 h at 375 rpm. The solvent was then evaporated by microwave radiation at low power using an LG domestic device (model MS1147X) in periods of 30 to 40 s, reaching a temperature of 70°C. The precursor material was dried at 200°C for 8 h and then calcined at 600°C in air for 5 h, at a heating rate of 100°C/h. The calcination was carried out in a programmable muffle with temperature control (Vulcan 3–550). Figure 1 shows the steps followed to obtain $NiSb_2O_6$ powders.

2.2. Physical Characterization of $NiSb_2O_6$ Powders. The identification of the $NiSb_2O_6$ phase was carried out at room temperature by means of powder X-ray diffraction using Siemens D500 equipment with CuKα radiation ($\lambda = 1518$ nm). The continuous scanning range 2θ was of 10 to 60° with steps of 0.02°, lasting one second each step. Raman spectroscopy characterization was done using a Thermo Scientific DXR Raman microscope with a 633 nm excitation source. The Raman spectra were measured from 100 to 800 cm^{-1} at room temperature, with an exposure time of 60 seconds. The powders' morphology was observed through a field-emission scanning electron microscope (FE-SEM, Tescan MIRA 3 LMU system, 10 kV) in high-vacuum mode. For the identification of the nanostructures, a transmission electron microscope (TEM, JEOL JEM-2010) in image-mode with an accelerating voltage of 200 kV was employed.

2.3. Pellet Preparation for the Gas Response Analysis. For testing in propane (C_3H_8) and carbon monoxide (CO) atmospheres, pellets of the material's powders were made compacting them by means of a hydraulic press (Simplex Ital Equip-25 Tons). The pellets had a diameter of 12 mm and a thickness of 500 μm.

The pellets' electrical resistance was measured at C_3H_8 and CO concentrations of 0, 5, 50, 100, 200, 300, 400, and 500 ppm, at temperatures of 23 (ambient), 100, 200, and 300°C. Their gas response (S) was calculated by the relative difference of the electric conductance (the reciprocal of the electric resistance), according to the expression [5, 11–14]: $S = (G_G - G_O)/G_O$, where G_G and G_O are the pellets' electrical conductance in the gases (C_3H_8 or CO) and in the air, respectively. The conductance was recorded by means of a Keithley digital multimeter (model 2001) as a function of the operating temperature and the concentration of the tested gas.

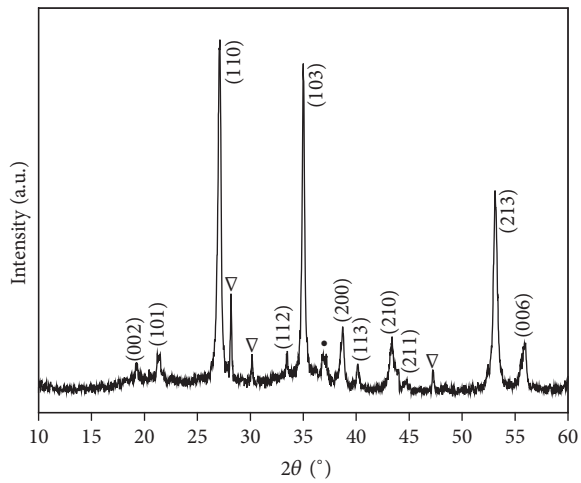

FIGURE 2: X-ray diffraction pattern of $NiSb_2O_6$ powders (at 600°C) synthesized by the microwave-assisted colloidal method.

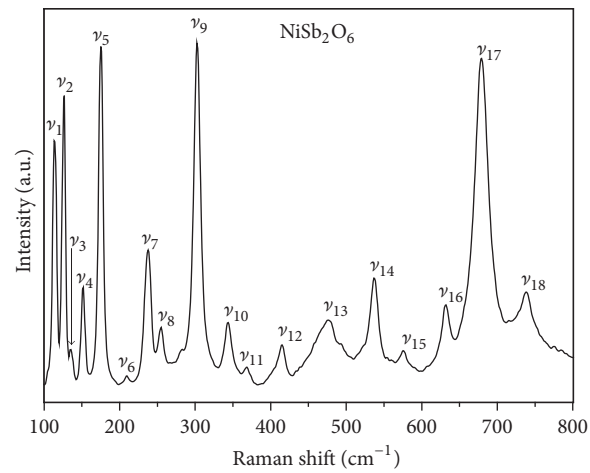

FIGURE 3: Raman spectrum of the $NiSb_2O_6$ powders calcined at 600°C, analyzed in air.

3. Results and Discussion

3.1. XRD Analysis. The X-ray diffraction pattern of the calcined material at 600°C is shown in Figure 2. The presence of the main phase corresponding to the $NiSb_2O_6$ is verified. The oxide was identified through the JCPDF card-file 38-1083. According to this, the oxide belongs to the materials with a trirutile-like structure [16], crystallizing with a space group $P4_2/mnm$ (136) [17–21] and cell parameters $a = 4.641$ Å and $c = 9.223$ Å. The width of the peaks in the diffractogram is indicative of a small particle size with a low noise level, which means a sample with high crystallinity [22]. Small portions of other materials outside the main phase can be also identified: SbO_2 (card-file 65-2446) located at the points 28.0°, 30.3°, and 47.3° and NiO located at 37.0° (card-file 65-2901). The crystal size (t) was estimated using Scherrer's equation [13] and the XRD-peaks (Figure 2):

$$t = \frac{0.9\lambda}{\beta \cos\theta}, \quad (1)$$

where λ is the radiation-wavelength (1518 nm), θ is the Bragg angle, and β is the full width at half maximum (FWHM) of the diffraction peak. All peaks of the main phase of the trirutile-like structure were considered, finding an average crystal size of about 31.19 nm.

According to the results shown in Figure 2, the synthesis of the oxide $NiSb_2O_6$ using the microwave-assisted colloidal method was successful. Several other authors have synthesized trirutile-type oxides following different synthesis processes [23]. Larcher et al. used precursor oxides MO (M = Cu, Ni, or Co) and Sb_2O_5 to synthesize the materials MSb_2O_6 at 800°C by means of the solid-state reaction method [24]. Ehrenberg et al. prepared the same oxide as Larcher et al. but at a temperature of 1450°C [16]. Comparing our results with those aforementioned, it was possible for us to obtain the $NiSb_2O_6$ at a significantly lower temperature following an alternative route of synthesis.

3.2. Raman Spectroscopy Analysis. The Raman spectroscopy results of the calcined powders are shown in Figure 3, where the bands ν_{14} to ν_{18}, in the range 500–800 cm^{-1}, correspond to the vibration of the Sb_2O_6 units of the oxide's crystals, and the bands ν_1 to ν_9, which are below 400 cm^{-1}, are due to the influence of Ni^{3+}. In detail, in the range 600–800 cm^{-1}, the stretching modes of the Sb-O_p bonds predominate, while, in the range 400–500 cm^{-1}, the deformation modes of the Sb-O_p bonds, coupled to the vibrations of the Ni-O bonds, are dominant. The 500–600 cm^{-1} bands are due to the elongation modes of the Sb-O_{cyc} bonds [19, 20]. This supports the results obtained by XRD.

3.3. SEM Analysis. Three SEM photomicrographs of the $NiSb_2O_6$ oxide's morphology are depicted in Figures 4(a)–4(c). The images were obtained at magnifications of 836x, 3.48kx, and 4.98kx, respectively. The insert in Figure 4(b) shows the size distribution histogram of the particles that comprise the microspheres.

The microstructure of the $NiSb_2O_6$ oxide calcined at 600°C is shown in Figure 4(a); it is observed that the material's surface is composed by the agglomeration of particles and the growth of microrods. The microrods appear on the entire material's surface, individually agglomerating at a single origin point and growing in different directions. The topography of this morphology is very fine (smooth) and appears to be solid; however, some microrods are hollow (see insert in Figure 4(a)). The microrods' dimensions were estimated at ~3.32 μm long and ~2.71 μm wide, while the length was measured in the range of 5 to 37 μm, with an average of ~10.56 μm and a standard deviation of ~5.4 μm. We reported in previous works that it is possible to obtain microrods of $CoSb_2O_6$ and $ZnSb_2O_6$ [15, 25], mesoporous nanoparticles of $CoSb_2O_6$ [14], nanorods of $MgSb_2O_6$ [26],

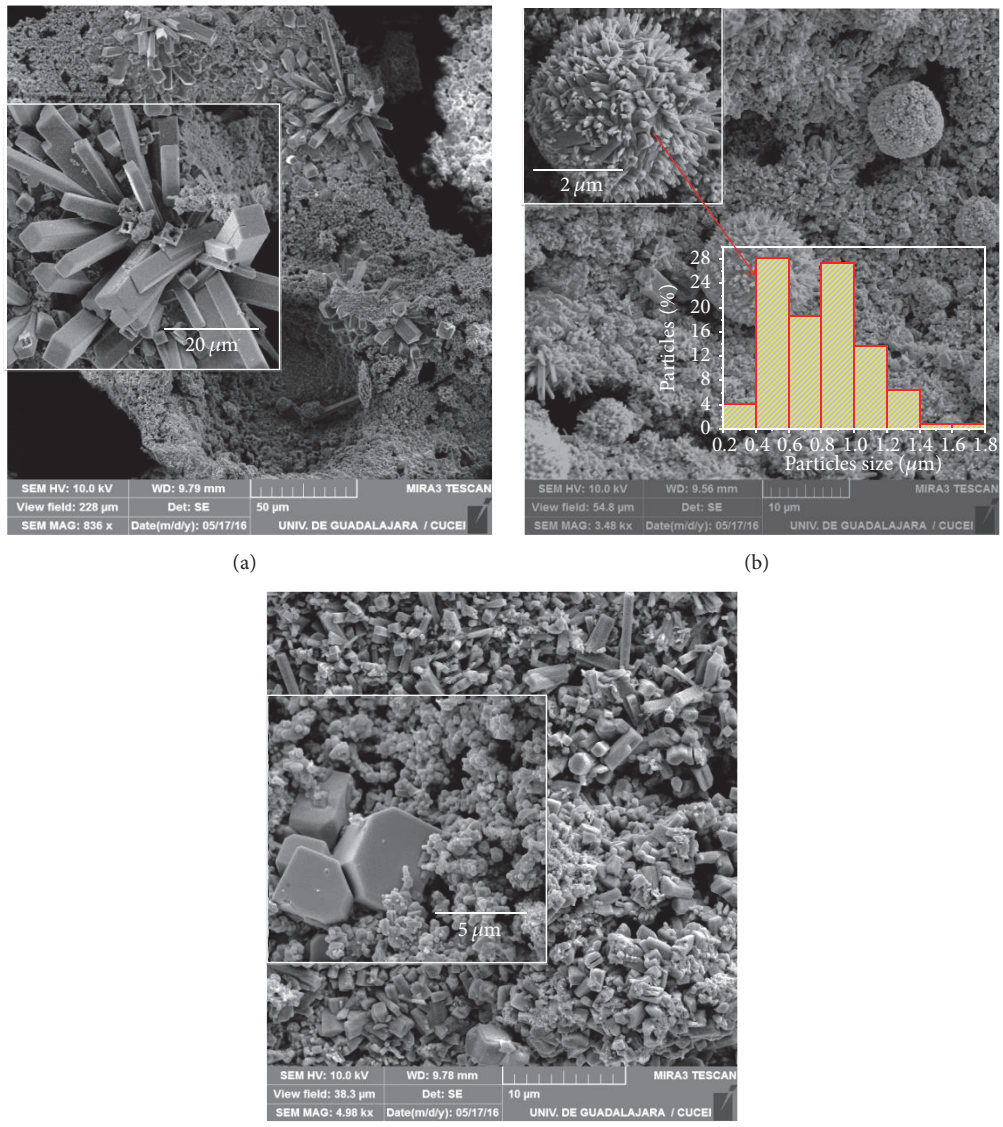

Figure 4: SEM images to magnifications: (a) 836x, (b) 3.48kx, and (c) 4.98kx; insert in Figure (b) microrods' particle size distribution.

and nanoparticles of $LaCoO_3$ [13], using different ethylenediamine concentrations during the synthesis of trirutile and perovskite-type materials by the colloidal method.

Another area of the material's surface is observed in Figure 4(b), where different sized microspheres can be identified. The average diameter of the spheres was estimated of ~8 μm. In the same image, it can be seen that the spheres are the result of the agglutination and agglomeration of particles, which take the surface of the sphere as a substrate. The size of the particles that comprise the spheres was calculated in the range of 0.22 to 1.8 μm, with an average of ~0.760 μm and a standard deviation of ~0.28 μm (see inserted histogram in Figure 4(b)). It has been reported in the literature that through the aerosol-route and by the Stöber method, it is possible to obtain different sized microspheres [27]. In our case, as already mentioned, the microspheres were obtained following an alternative method of synthesis: the colloidal method in presence of ethylenediamine. The microspheres formation is attributable not only to the effect of the temperature (when it was calcined at 600°C) but also to the coalescence of very fine particles present on the material's surface.

An additional point on the surface was analyzed. Figure 4(c) shows a surface composed of different particles, which grew agglomerated by the effect of temperature. Generally speaking, Figures 4(a)–4(c) show that these morphologies appeared commonly on the oxide's surface.

The growth of this type of microstructure is due to the fact that ethylenediamine produces coordinated compounds, such as the $NiSb_2O_6$, that are capable of modifying the microstructure and the particle size in transition metals [28–30]. In this case, the ethylenediamine is incorporated into the inorganic solid forming complexes, which join together after

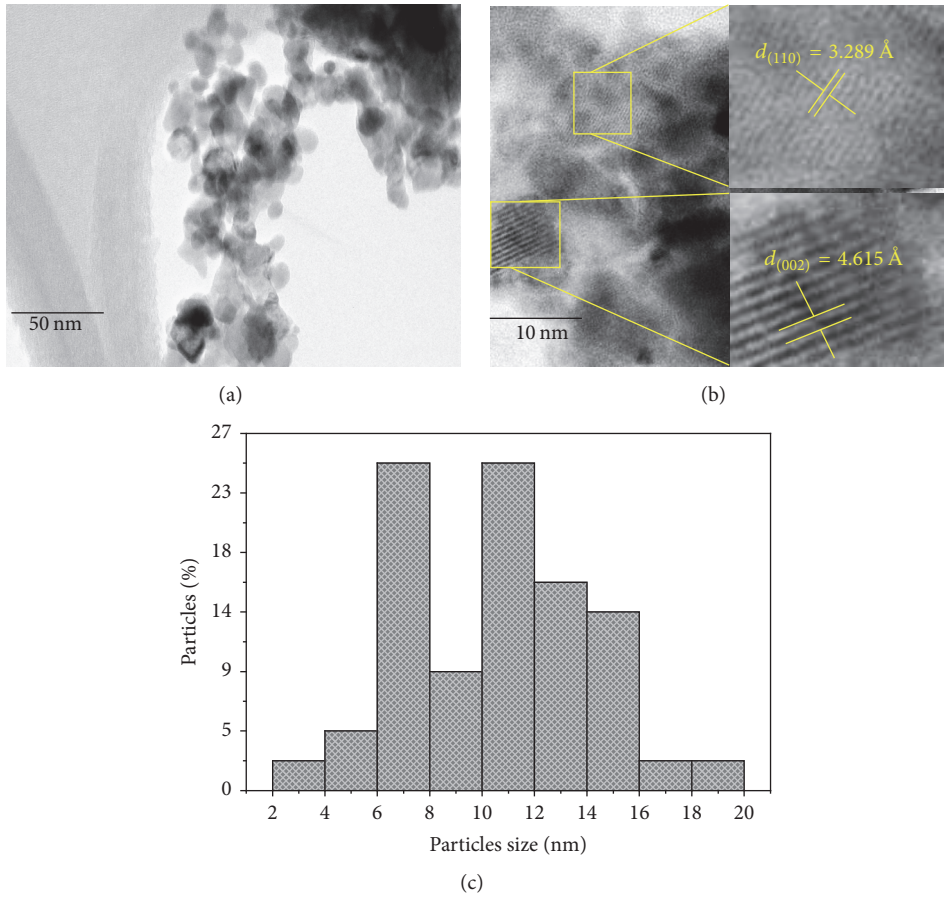

FIGURE 5: TEM images of the $NiSb_2O_6$ powders calcined at 600°C: (a) nanoparticles, (b) HRTEM image showing the nanoparticles' crystalline planes, and (c) nanoparticle-size distribution.

both the reaction and the heat treatment took place, giving rise to the formation of the microstructure shown in Figure 4.

The preparation of inorganic compounds using the colloidal method in presence of ethylenediamine has been discussed extensively in previous works [31, 32]. Some authors obtained similar morphologies to those presented here, reporting that by such synthesis method it is possible to have a better control during the particle nucleation and growth processes, producing materials with desirable morphologies [31–33]. Therefore, the microstructures obtained are in accordance with the crystallization criteria described by LaMer and Dinegar [14, 15, 25, 26, 34], which establish that the crystallization of stable nuclei provokes a strong chemical reaction (the colloidal dispersion), which makes it possible to obtain inorganic materials with different morphologies.

3.4. TEM Analysis. Two TEM images of the oxide are shown in Figures 5(a) and 5(b). Nanoparticles appearing on the $NiSb_2O_6$ surface are depicted in Figure 5(a); Figure 5(b) shows a high-resolution image (HRTEM) of the nanoparticles' surface; Figure 5(c) depicts a histogram of the nanoparticle-size distribution.

Different sized nanoparticles and a very homogeneous morphology can be observed in Figure 5(a). In addition, some nanoparticles were found on a microbase, taking it as a substrate for nucleation and growth. The high-resolution analysis (HRTEM) on a selected area of the nanoparticles (Figure 5(b)) revealed the formation of the material's crystalline planes, confirming the crystalline nature of the nanoparticles (see inserted figures). The distance between planes (d) was found in the range of ~3,289 to 4,615 Å, corresponding to the planes (110) and (002), respectively. These results support the X-ray diffraction analysis (Figure 2). Broadly speaking, the size of the nanoparticles was found in the range of 2 to 20 nm, with an average of ~10.7 nm and a standard deviation of ~3.4 nm (Figure 5(c)).

3.5. Sensing Properties Analysis. Figures 6(a) and 6(b) show the results of the response tests in gas propane, which reveals that the $NiSb_2O_6$ pellets are very sensitive to the test gas concentrations and the operating temperature: the material's response increases as the temperature and the C_3H_8 concentration rise. Increased response is caused by the increase in the number of gas molecules that react with oxygen on the material's surface. In addition, the oxide's response is associated with the effect of temperature, which increases during the tests [14]. The highest response recorded was ~1.125 corresponding to 500 ppm of propane, at a

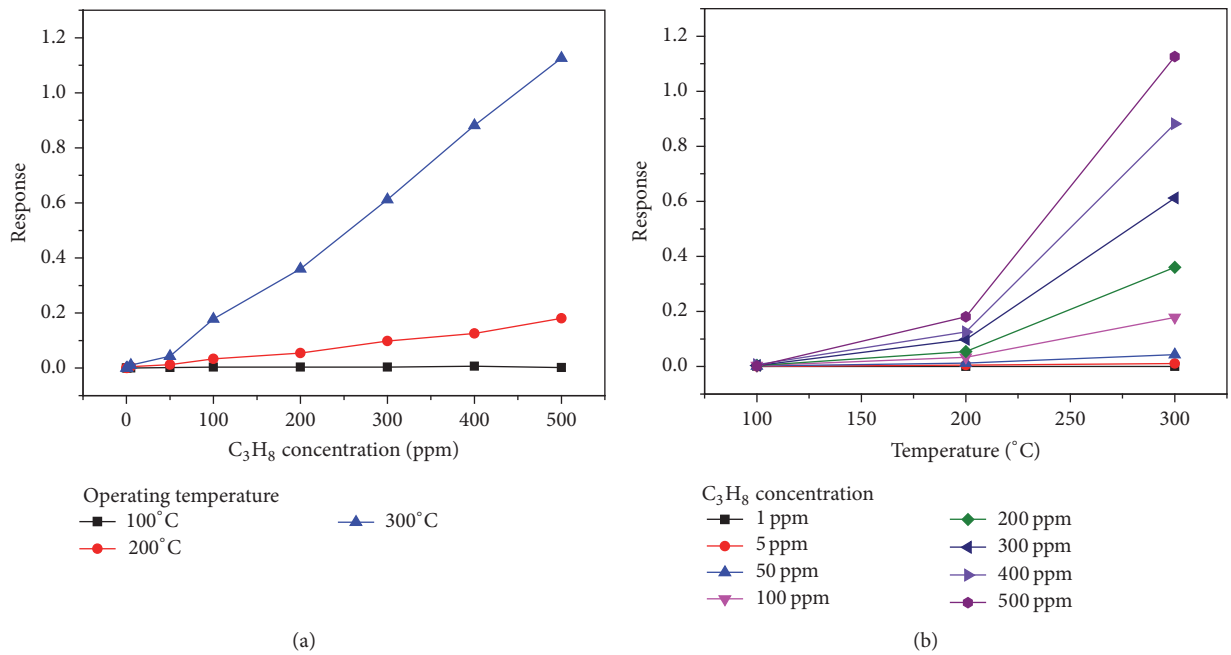

FIGURE 6: Response of $NiSb_2O_6$ nanoparticles as a function of: (a) C_3H_8 concentration and (b) operating temperature.

temperature of 300°C. At such temperature, the response values were 0, 0.0105, 0.0436, 0.178, 0.360, 0.6123, 0.881, and 1.125 at concentrations 1, 5, 50, 100, 200, 300, 400, and 500 ppm, respectively. However, at temperatures below 200°C there were no changes in the material's electrical resistance because the terminal energy is not enough to produce the oxygen-desorption reaction [35], regardless of the propane concentration [13]. These results are consistent with similar oxides that have been tested in propane atmospheres [11–14, 25, 26].

The gas sensing mechanism is based on the change of the electrical resistance (or conductance) due to the adsorption and desorption of oxygen on the $NiSb_2O_6$ pellets' surface. When the oxygen species adsorb on the surface, the material undergoes changes in its conductance, provoking the formation of the electron depletion layer, thus resulting in changes in the response of the oxide [36]. The chemical reaction between the surface of a semiconductor material and propane has been discussed in previous works [37, 38]. In our case, the reaction may be the one reported in [36, 39]: $C_3H_8 + 10O_2^- \rightarrow 3CO_2 + 4H_2O + e^-$.

The results of tests in CO atmospheres at different concentrations and temperatures are presented in Figures 7(a) and 7(b). As in the propane experiments, the $NiSb_2O_6$ pellets showed a good response by raising the temperature and the CO concentration. However, at temperatures below 200°C, there were no changes in the electrical resistance regardless of the CO concentration. In contrast, when the temperature increased from 200 to 300°C, the response increased significantly. Apparently, the response of the material is associated with the increase of the oxygen adsorbed on the material's surface at high temperatures [13, 35]. Chang [35] and Balamurugan et al. [40] report that the adsorption of different oxygen species on the sensor's surface depends on the operating temperature [41, 42]. Therefore, when the tests were performed at temperatures below 200°C, the oxygen species were mainly O_2^-; on the other hand, by raising the temperature to 300°C, the oxygen species that are chemically adsorbed are O^- and O^{2-}, which signifies changes in the electrical resistance and, consequently, an increase in the response of the $NiSb_2O_6$. The maximum response obtained was of ~2.14 at 300°C for 300 ppm of CO. Other values at the same temperature were 0.013, 0.109, 0.321, 0.482, 1.25, and 2.14.

In order to discern the best conditions for a maximum performance of the $NiSb_2O_6$ nanoparticles in C_3H_8 and CO atmospheres, Figure 8 shows a graph of response versus concentration of both gases at a temperature of 300°C. According to these results, the response of the nanoparticles is clearly dependent on the temperature and the concentration of the test gases [42, 43]. The optimum operating temperature of the oxide was of 300°C for both gases, and the best response was recorded in the CO atmosphere at a concentration of 300 ppm. This trend is associated with the fact that during the tests in CO atmospheres, the surface of the pellets was enriched with oxygen species, giving rise to a greater response in this atmosphere. Therefore, the $NiSb_2O_6$ oxide possesses a high selectivity in CO concentrations.

These results were compared with those for similar oxides tested also in C_3H_8 and CO atmospheres. For example, SnO_2 showed in [11] maximum responses of ~0.4 and ~0.6 at concentrations of 100 and 500 ppm of propane at 300°C, respectively. In our case, the highest response was of ~1.125 at a C_3H_8 concentration of 500 ppm and of ~2.14 at a CO concentration of 300 ppm, both at 300°C. In addition, we have previously reported [14, 15, 25, 27] that the trirutile-type

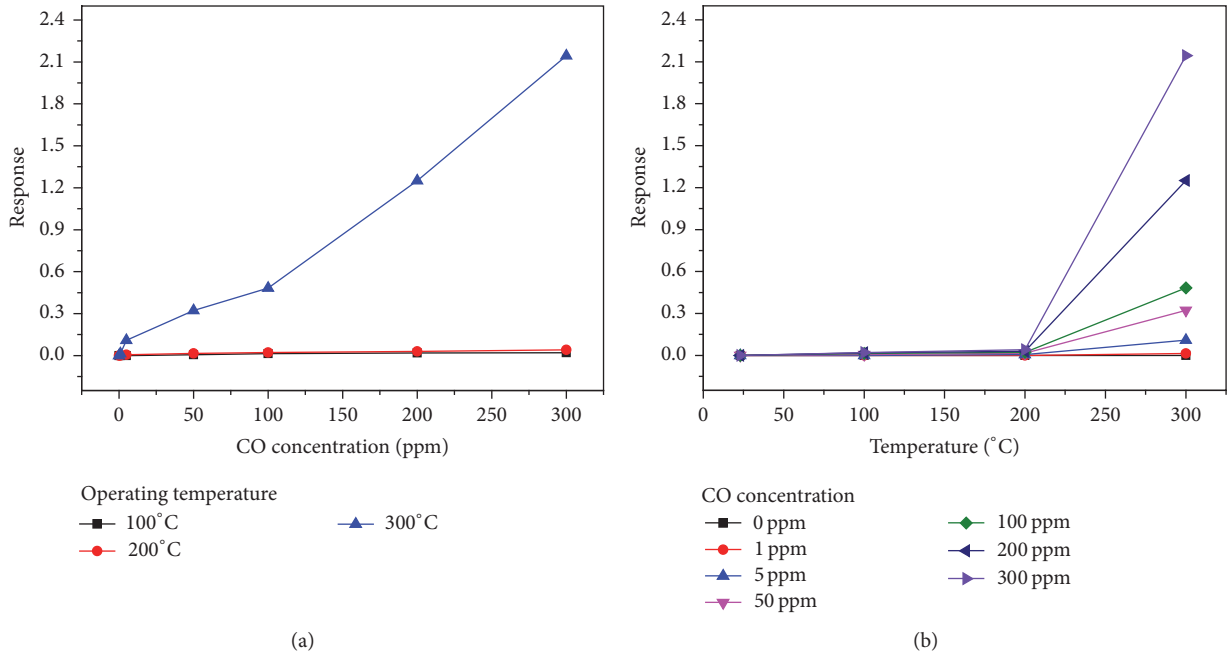

FIGURE 7: Response of the $NiSb_2O_6$ nanoparticles to (a) carbon monoxide concentration and (b) operating temperatures.

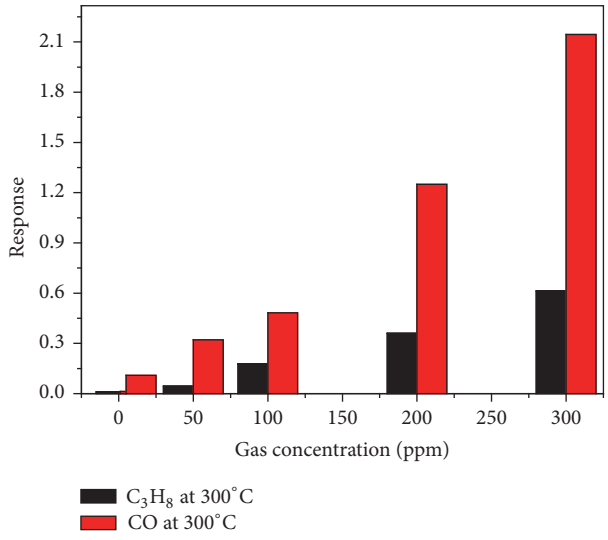

FIGURE 8: Response of $NiSb_2O_6$ nanoparticles to different concentrations of C_3H_8 and CO at 300°C.

oxides $CoSb_2O_6$, $ZnSb_2O_6$, and $MgSb_2O_6$ have good thermal stability in CO, CO_2, and C_3H_8 atmospheres. Therefore, pellets made with $NiSb_2O_6$ nanoparticles may be excellent candidates for using them as gas detectors, particularly in CO and C_3H_8 atmospheres.

4. Conclusions

Micro- and nanoparticles of trirutile-type $NiSb_2O_6$ were synthesized using the microwave-assisted colloidal method. This synthesis route is economically very suitable and allows good fabrication efficiency because it makes it possible to have an excellent control of the morphology and the particle size. It was found that $NiSb_2O_6$ nanoparticles are highly sensitive to various concentrations of C_3H_8 and CO, operating at relatively low temperatures. The oxide's response increases directly proportional to the temperature and the concentrations of the test gases, obtaining a very good response in both gases. Due to the above, $NiSb_2O_6$ with trirutile-type structure is a great candidate to be used as a gas sensor.

Conflicts of Interest

The authors declare that there are no conflicts of interest regarding the publication of this paper.

Acknowledgments

Alex Guillén Bonilla thanks the Mexico's National Council of Science and Technology *(CONACyT)* for the financial support granted to make this work. Also worth noting is the technical assistance received from Sergio Oliva-León *(U. de G.)*, Miguel-Ángel Luna-Arias, Lorenzo Gildo Ortiz, and Jaime Santoyo Salazar *(CINVESTAV)*. This work was partially funded by the *CONACYT's* "Retention Project" no. 263656, by *CONACyT's* "Thematic Network Project" no. 271872, by *CONACyT's* "Frontiers of Science Project" no. 1103, and by PRODEP 2016 Project no. F-PROMEP-39/Rev-04 SEP-23-005 (no. DSA/103.5/16/10313).

References

[1] M. Fleischer and H. Meixner, "Fast gas sensors based on metal oxides which are stable at high temperatures," *Sensors and Actuators B: Chemical*, vol. 43, no. 1–3, pp. 1–10, 1997.

[2] P. T. Moseley, "Materials selection for semiconductor gas sensors," *Sensors and Actuators: B. Chemical*, vol. 6, no. 1-3, pp. 149–156, 1992.

[3] K. Wetchakun, T. Samerjai, and N. Tamaekong, "Semiconducting metal oxides as sensors for environmentally hazardous gases," *Sensors and Actuators B: Chemical*, vol. 160, no. 1, pp. 580–591, 2011.

[4] X. Y. Xue, Y. J. Chen, Y. G. Liu, S. L. Shi, Y. G. Wang, and T. H. Wang, "Synthesis and ethanol sensing properties of indium-doped tin oxide nanowires," *Applied Physics Letters*, vol. 88, no. 20, Article ID 201907, 2006.

[5] G. Carbajal-Franco, A. Tiburcio-Silver, J. M. Domínguez, and A. Sánchez-Juárez, "Thin film tin oxide-based propane gas sensors," *Thin Solid Films*, vol. 373, no. 1-2, pp. 141–144, 2000.

[6] C. Wang, L. Yin, L. Zhang, D. Xiang, and R. Gao, "Metal oxide gas sensors: sensitivity and influencing factors," *Sensors*, vol. 10, no. 3, pp. 2088–2106, 2010.

[7] S. Park, H. Kheel, G.-J. Sun, T. Ko, W. I. Lee, and C. Lee, "Acetone gas sensing properties of a multiple-networked Fe2O3-functionalized CuO nanorod sensor," *Journal of Nanomaterials*, vol. 2015, Article ID 830127, 2015.

[8] Q. Wang, N. Yao, C. Liu et al., "Synthesis of Hollow $ZnSnO_3$ nanospheres with high ethanol sensing properties," *Journal of Nanomaterials*, vol. 2016, Article ID 2381823, 5 pages, 2016.

[9] M. Devetak, B. Berčič, M. Uplaznik, A. Mrzel, and D. Mihailovic, "Mo6S3i6 nanowire network vapor pressure chemisensors," *Chemistry of Materials*, vol. 20, no. 5, pp. 1773–1777, 2008.

[10] Z. Deng, X. Fang, D. Li et al., "Room temperature ozone sensing properties of p-type transparent oxide CuCrO2," *Journal of Alloys and Compounds*, vol. 484, no. 1-2, pp. 619–621, 2009.

[11] H. Gómez-Pozos, J. L. González-Vidal, and G. A. Torres, "Chromium and ruthenium-doped zinc oxide thin films for propane sensing applications," *Sensors*, vol. 13, no. 3, pp. 3432–3444, 2013.

[12] H. Gómez-Pozos, J. L. González-Vidal, G. A. Torres, M. de la Luz Olvera, and L. Castañeda, "Physical characterization and effect of effective surface area on the sensing properties of tin dioxide thin solid films in a propane atmosphere," *Sensors*, vol. 14, no. 1, pp. 403–415, 2013.

[13] L. Gildo-Ortiz, H. Guillén-Bonilla, J. Santoyo-Salazar et al., "Low-temperature synthesis and gas sensitivity ofperovskite-type $LaCoO_3$ nanoparticles," *Journal of Nanomaterials*, vol. 2014, Article ID 164380, 8 pages, 2014.

[14] H. Guillén-Bonilla, L. Gildo-Ortiz, M. L. Olvera-Amador et al., "Sensitivity of mesoporous $CoSb_2O_6$ nanoparticles to gaseous CO and C_3H_8 at low temperatures," *Journal of Nanomaterials*, vol. 2015, Article ID 308465, 9 pages, 2015.

[15] A. Guillén-Bonilla, V.-M. Rodríguez-Betancourtt, M. Flores-Martínez et al., "Dynamic response of $CoSb_2O_6$ trirutile-type oxides in a CO_2 atmosphere at low-temperatures," *Sensors*, vol. 14, no. 9, pp. 15802–15814, 2014.

[16] H. Ehrenberg, G. Wltschek, J. Rodriguez-Carvajal, and T. Vogt, "Magnetic structures of the tri-rutiles NiTa2O6 and NiSb2O6," *Journal of Magnetism and Magnetic Materials*, vol. 184, no. 1, pp. 111–115, 1998.

[17] J. N. Reimers, J. E. Greedan, and M. A. Subramanian, "Crystal structure and magnetism in MnSb2O6: Incommensurate long-range order," *Journal of Solid State Chemistry*, vol. 79, no. 2, pp. 263–276, 1989.

[18] D. Reinen, M. Atanasov, and S.-L. Lee, "Second-sphere ligand field effects on oxygen ligator atoms and experimental evidence - The transition metal-oxygen bond in oxidic solids," *Coordination Chemistry Reviews*, vol. 175, no. 1, pp. 91–158, 1998.

[19] H. Haeuseler, "Infrared and Raman spectra and normal coordinate calculations on trirutile-type compounds," *Spectrochimica Acta Part A: Molecular Spectroscopy*, vol. 37, no. 7, pp. 487–495, 1981.

[20] E. Husson, Y. Repelin, H. Brusset, and A. Cerez, "Spectres de vibration et calcul du champ de force des antimoniates et des tantalates de structure trirutile," *Spectrochimica Acta Part A*, vol. 35, no. 10, pp. 1177–1187, 1979 (French).

[21] A. Singh, A. Singh, S. Singh, and P. Tandon, "Nickel antimony oxide (NiSb2O6): A fascinating nanostructured material for gas sensing application," *Chemical Physics Letters*, vol. 646, pp. 41–46, 2016.

[22] E. Delgado and C. R. Michel, "CO_2 and O_2 sensing behavior of nanostructured barium-doped $SmCoO_3$," *Materials Letters*, vol. 60, no. 13-14, pp. 1613–1616, 2006.

[23] V. Samuel, A. B. Gaikwad, A. D. Jadhav, N. Natarajan, and V. Ravi, "A coprecipitation technique to prepare NiNb2O6," *Materials Letters*, vol. 61, no. 11-12, pp. 2354-2355, 2007.

[24] D. Larcher, A. S. Prakash, L. Laffont et al., "Reactivity of antimony oxides and MSb_2O_6 (M = Cu, Ni, Co), trirutile-type phases with metallic lithium," *Journal of the Electrochemical Society*, vol. 153, no. 9, pp. A1778–A1787, 2006.

[25] H. Guillen-Bonilla, V.-M. Rodríguez-Betancourtt, J.-T. Guillén-Bonilla et al., "CO and C3H8 sensitivity behavior of zinc antimonate prepared by a microwave-assisted solution method," *Journal of Nanomaterials*, vol. 2015, Article ID 979543, 2015.

[26] H. Guillén-Bonilla, M. Flores-Martínez, V.-M. Rodríguez-Betancourtt et al., "A novel gas sensor based on MgSb2O6 nanorods to indicate variations in carbon monoxide and propane concentrations," *Sensors (Switzerland)*, vol. 16, no. 2, article no. 177, 2016.

[27] A. Bystr, B. H, B. Mason, A. Byström, and B. Hök, "The crystal structure of zinc metantimonate and similar compounds," *Arkiv Kemi Mineral Geology*, vol. 15B, no. 4, pp. 1–8, 1941.

[28] V. V. Gorbunov, A. A. Shidlovskii, and L. F. Shmagin, "Combustion of transition-metal ethylenediamine nitrates," *Combustion, Explosion, and Shock Waves*, vol. 19, no. 2, pp. 172-173, 1983.

[29] Z.-X. Deng, C. Wang, X.-M. Sun, and Y.-D. Li, "Structure-directing coordination template effect of ethylenediamine in formations of ZnS and ZnSe nanocrystallites via solvothermal route," *Inorganic Chemistry*, vol. 41, no. 4, pp. 869–873, 2002.

[30] X. Wang and Y. Li, "Solution-based synthetic strategies for 1-D nanostructures," *Inorganic Chemistry*, vol. 45, no. 19, pp. 7522–7534, 2006.

[31] E. Matijević, "Preparation and properties of uniform size colloids," *Chemistry of Materials*, vol. 5, no. 4, pp. 412–426, 1993.

[32] E. Matijevic, "Uniform inorganic colloid dispersions. Achievements and challenges," *Langmuir*, vol. 10, no. 1, pp. 8–16, 1994.

[33] A. Chittofrati and E. Matijević, "Uniform particles of zinc oxide of different morphologies," *Colloids and Surfaces*, vol. 48, no. C, pp. 65–78, 1990.

[34] V. K. Lamer and R. H. Dinegar, "Theory, production and mechanism of formation of monodispersed hydrosols," *Journal of the American Chemical Society*, vol. 72, no. 11, pp. 4847–4854, 1950.

[35] S. C. Chang, "Oxygen chemisorption on tin oxide: correlation between electrical conductivity and EPR measurements," *Journal of Vacuum Science & Technology*, vol. 17, no. 1, pp. 366–369, 1979.

[36] V. K. Jayaraman, A. Maldonado Álvarez, and M. De la Luz Olvera Amador, "A simple and cost-effective zinc oxide thin film sensor for propane gas detection," *Materials Letters*, vol. 157, Article ID 18958, pp. 169–171, 2015.

[37] M. Kerlau, P. Reichel, N. Bârsan, U. Weimar, S. Delsarte-Guéguen, and O. Merdrignac-Conanec, "Detection of propane by "GaON" thick-film gas sensors," *Sensors and Actuators, B: Chemical*, vol. 122, no. 1, pp. 14–19, 2007.

[38] D. Koziej, N. Bârsan, V. Hoffmann, J. Szuber, and U. Weimar, "Complementary phenomenological and spectroscopic studies of propane sensing with tin dioxide based sensors," *Sensors and Actuators, B: Chemical*, vol. 108, no. 1-2, pp. 75–83, 2005.

[39] J. K. Srivastava, P. Pandey, V. N. Mishra, and R. Dwivedi, "Sensing mechanism of Pd-doped SnO2 sensor for LPG detection," *Solid State Sciences*, vol. 11, no. 9, pp. 1602–1605, 2009.

[40] C. Balamurugan, A. R. Maheswari, and D.-W. Lee, "Structural, optical, and selective ethanol sensing properties of p-type semiconducting CoNb2O6 nanopowder," *Sensors and Actuators, B: Chemical*, vol. 205, pp. 289–297, 2014.

[41] L. Gildo-Ortiz, J. Reyes-Gómez, J. Flores-Álvarez et al., "Synthesis, characterization and sensitivity tests of perovskite-type $LaFeO_3$ nanoparticles in CO and propane atmospheres," *Ceramics International*, vol. 24, no. 16, pp. 18821–18827, 2016.

[42] J. Morán-Lázaro, F. López-Urías, E. Muñoz-Sandoval et al., "Synthesis, Characterization, and Sensor Applications of Spinel $ZnCo_2O_4$ Nanoparticles," *Sensors*, vol. 16, no. 12, p. 2162, 2016.

[43] X. Zhao, R. Zhou, Q. Hua, L. Dong, R. Yu, and C. Pan, "Recent Progress in Ohmic/Schottky-Contacted ZnO Nanowire Sensors," *Journal of Nanomaterials*, vol. 2015, Article ID 854094, 2015.